LA-UR-23-29674
Accepted Manuscript

Assessment of the literature about Be-W mixed material layer formation in the fusion reactor environment

Lasa, Ane
Dasgupta, Dwaipayan
Baldwin, Matthew J
Cusentino, Mary Alice
Hatton, Peter John
Uberuaga, Blas P.
Yang, Li
Wirth, Brian D

Provided by the author(s) and the Los Alamos National Laboratory (2024-06-27).

To be published in: Materials Research Express

DOI to publisher's version: 10.1088/2053-1591/ad2c3c

Permalink to record:
https://permalink.lanl.gov/object/view?what=info:lanl-repo/lareport/LA-UR-23-29674

Materials Research Express

TOPICAL REVIEW • OPEN ACCESS

Assessment of the literature about Be-W mixed material layer formation in the fusion reactor environment

To cite this article: Ane Lasa *et al* 2024 *Mater. Res. Express* **11** 032002

IOP Publishing Mater. Res. Express 11 (2024) 032002 https://doi.org/10.1088/2053-1591/ad2c3c

Materials Research Express

CrossMark

OPEN ACCESS

RECEIVED
21 August 2023

REVISED
23 October 2023

ACCEPTED FOR PUBLICATION
22 February 2024

PUBLISHED
1 March 2024

TOPICAL REVIEW

Assessment of the literature about Be-W mixed material layer formation in the fusion reactor environment

Ane Lasa[1,*], Dwaipayan Dasgupta[1,*], Matthew J Baldwin[2], Mary Alice Cusentino[3], Peter Hatton[4], Danny Perez[5], Blas P Uberuaga[4], Li Yang[1] and Brian D Wirth[1,6]

[1] Department of Nuclear Engineering, University of Tennessee, Knoxville, TN 37996, United States of America
[2] Center for Energy Research, University of California, San Diego, La Jolla, CA 92093, United States of America
[3] Material, Physical, and Chemical Sciences Center, Sandia National Laboratories, Albuquerque, NM, 87123, United States of America
[4] Materials Science and Technology Division MST-8, Los Alamos National Laboratory, Los Alamos, NM, 87545, United States of America
[5] Theoretical Division T-1, Los Alamos National Laboratory, Los Alamos, NM, 87545, United States of America
[6] Fusion Energy Division, Oak Ridge National Laboratory, Oak Ridge, TN 37830, United States of America
[*] Authors to whom any correspondence should be addressed.

E-mail: aesquisa@utk.edu and ddasgupta@utk.edu

Keywords: material-mixing, tungsten, beryllium, literature review

Abstract

All plasma facing surfaces in a fusion reactor, whether initially pure or an alloy, will rapidly evolve into a mixed material due to plasma-induced erosion, migration and redeposition. Beryllium (Be) erosion from the main chamber, and its transport and deposition on to a tungsten (W) divertor results in the growth of mixed Be-W layers, which can evolve to form beryllides. These Be-W mixed materials exhibit generally less desirable properties than pure tungsten or pure beryllium, such as lower melting points. In order to better understand the parameter space for growth of these alloys, this paper reviews the literature on Be-W mixed material formation experiments—in magnetically confined fusion reactors, in linear plasma test stands, and during thin-film deposition—and on computational modeling of Be-W interactions, as well as briefly assesses the Be-W growth kinetics. We conclude that the following kinetic steps drive the material mixing: adsorption of the implanted/deposited ion on the metal surface; diffusion of the implanted/deposited ion from surface into the bulk, which is accelerated by defects; and loss of deposited material through erosion. Adsorption dominates (or prevents) material mixing in thin-film deposition experiments, whereas diffusion drives material mixing in plasma exposures due to the energetic ion implantation.

1. Introduction

All plasma facing surfaces in a fusion reactor, whether initially pure or a compound, will rapidly evolve into a mixed material due to plasma-induced erosion, migration and redeposition. These mixed materials exhibit different properties than the initial plasma facing material or a linear mixture of their elements. These changes have important implications for the predictability of the component erosion and fuel retention within these layers, the performance and reliability of the mixed-material PFCs, and safety of the components.

Current fusion devices and some future reactor designs (e.g. Joint European Torus (JET) and initially planned for ITER) often combine a low-Z material such as beryllium (Be) for the main chamber with a high-Z material such as tungsten (W) for the divertor. This combination places low-Z materials, which radiate less if they are eroded and transported into the core, in areas that come closest to the confined plasma (e.g. limiters); and high-Z materials, which better handle large particle and heat fluxes, in areas of most extreme heat and particle flux conditions (e.g. divertor). Beryllium erosion, transport and deposition on to the tungsten divertor (most common impurity migration pattern in the scrape-off-layer plasma of a tokamak) results in the growth of mixed Be-W layers, as shown in figure 1.

It is unique that tungsten (a transition metal) and beryllium (the smallest alkaline earth metal) - two metals with disparate physicochemical properties—form ordered stoichiometric alloys. Among all the metals, tungsten

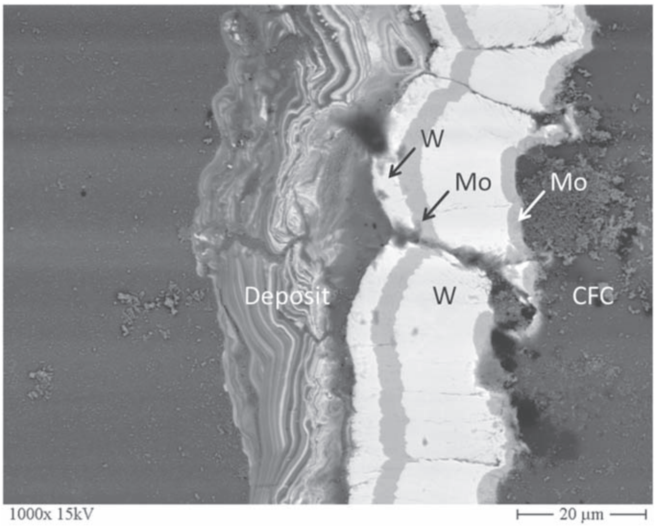

Figure 1. Material redeposited on the JET ILW tungsten divertor tile 1, mainly composed of beryllium. Reproduced courtesy of IOP Publishing. Figure (6) from [1]. Copyright (2016) IOP Publishing.

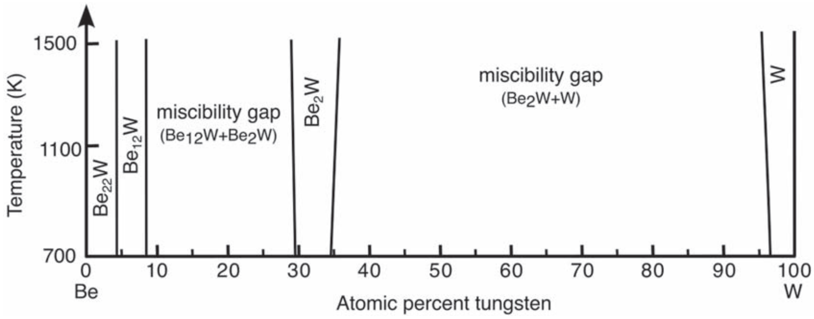

Figure 2. The Be-W binary phase diagram showing three stable intermetallic phases, and large miscibility gaps. Figure adapted from figure 1 of [7], with the temperature limited to the range of interest, i.e, 700-1500 K. Reuse permitted by Springer Nature. Copyright (1986) Springer Nature.

has the highest melting point and cohesive energy, and both the values for beryllium are on the lower end of the spectrum. Bulk tungsten has a bcc structure with an atomic radius of 0.1442 nm [2] and melting point of 3687 K [3]. In contrast, beryllium has an hcp structure with an atomic radius of 0.1113 nm [2] and melting point of 1560 K [4]. The cohesive energy of beryllium is 3.71 eV [5] and the in-plane nearest neighbor is at a longer distance (2.279 Å per density functional theory (DFT), and 2.287 Å per experiments [6]) than the interplanar distance (DFT 2.191 Å [3], experiment 2.226 Å [6]). For bcc tungsten, DFT calculations indicate a lattice constant of 3.186 Å (experimental: 3.155 Å) [3] and a cohesive energy of 9.01 eV, which is consistent with its high melting point.

The intermixing of tungsten and beryllium due to surface erosion and impurity migration drives the formation of mixed Be-W materials, which can evolve to form tungsten beryllides. The three stable alloy compositions are $Be_{22}W$, $Be_{12}W$ and Be_2W [7], as shown in the equilibrium phase diagram in figure 2, and have narrow phase widths, meaning they prefer to form as nearly stoichiometric compounds. There exist large miscibility gaps between the two most stable intermetallic phases, $Be_{12}W$ and Be_2W, and between the most tungsten rich intermetallic phase (Be_2W) and pure tungsten [7]. These tungsten beryllide alloys exhibit different (and generally less desirable) properties than pure tungsten or pure beryllium. For example, Doerner *et al* [8] report melting of the tungsten crucible that holds hot beryllium, due to inter-mixing of the two elements and formation of a low-melting point eutectic compound. The approximate melting points for intermetallics are in between that for tungsten and beryllium, 2523 K and 2023 K for Be_2W and $Be_{12}W$, respectively [4]. The cohesive energy follows a similar trend and it is reported as 5.591eV and 4.190 eV for Be_2W and $Be_{12}W$, respectively. Gyoeroek and coworkers observed a nearly linear relation between the cohesive energy calculated by DFT and the Be:W ratio [3].

With the objective of better understanding the parameter space for the formation of different Be-W alloys, this paper reviews experiments in magnetically confined fusion reactors, linear plasma test stand devices, and thin-film deposition experiments, as well as modeling work on Be-W mixed material formation. Thin-film deposition growth, in addition to plasma confinement and linear plasma devices, provide three distinctive mixed-material growth environments. For instance, material is deposited at low ion energies (e.g. <1 eV for deposition during molecular beam epitaxial growth in thin-film experiments [9]), whereas it is energetically implanted during plasma exposure. Further, material is deposited in its pure form during thin-film growth, but it is generally a seeded impurity (concentrations of $<O(1\%)$) during plasma exposure. The environmental conditions in magnetic confinement fusion reactors and linear plasma facilities also differ significantly. Ion impacts are approximately mono-energetic and their trajectories nearly normal to the surface in linear plasma experiments; whereas ion incidence follows a broad energy distribution and occurs at shallow angles in confinement facilities. Further, plasma in confinement facilities contains a range of intrinsic and extrinsic impurities, while the plasma composition is well controlled in linear plasma experiments. Therefore, the article is structured to reflect these three distinct environments. After this brief introduction, we present the Be-W mixing experiments organized into 3 main sections: thin-film deposition experiments are presented in section 2; linear (non-confinement) plasma device experiments are discussed in section 3 and magnetic confinement fusion reactor (specifically tokamak) experiments are summarized in section 4. Sections 2 and 3 first summarize the main findings of papers available in the literature, followed by a discussion of the results, including comparison across similar work and their of possible commonalities, generalizations and discrepancies. We also look for possible explanations behind these differences, and describe how the experiments fit the broader literature. Section 5 summarizes the atomic scale modeling of Be-W interactions and section 6 discusses the experimental findings in sections 2- 4 based on the computational understanding of the system presented in section 5. We finalize the paper with a summary of the mechanisms that drive or inhibit material mixing in different environments and with a discussion of the outstanding issues remaining to be solved in order to predict hydrogen isotope retention in mixed Be-W plasma facing components.

2. Thin-film deposition experiments

2.1. Results from film deposition experiments

A group of articles by Wiltner and Linsmeier [2, 10–12] describe the experiments performed by the authors, in which beryllium films were vapor deposited onto W with subsequent annealing, and a 200 nm tungsten film was deposited on beryllium in a magnetron sputter device. These experiments were performed at room temperature with subsequent annealing up to 1070 K.

From the set of experiments the authors conclude that Be_2W forms during beryllium deposition experiments, although the mixed material layer is restricted to the film-substrate interface. The residual beryllium layer thicknesses are limited to 1.2–1.6 nm (depending on initial deposited layer thickness). Their rationale is that the final stoichiometric Be_2W is only reached during the annealing of beryllium layers on tungsten, but requires temperatures of at least 970 K. However, at these temperatures beryllium is known to thermally evaporate. Beryllium diffusion into the tungsten bulk is not observed.

In contrast, during tungsten deposition experiments, the $Be_{12}W$ alloy forms within the entire diffusion depth, with a tungsten diffusion coefficient of $D = 1.6 \times 10^{-13}$ cm^2 s^{-1}, but only after annealing at $T > 1000$ K [11, 13]. This temperature does not lead to evaporation of tungsten. The authors provide a detailed analysis of the composition (alloy vs.metallic) and elemental (W, Be, O..) depth profiles. Additionally, Linsmeier *et al* [13] published a simplified reaction front model (RFM), which they applied to XPS experiments of Be-W alloy formation. The article also provides a good review of the literature on Be-W mixed material formation experiments (up until 2007).

Similarly, Bauer and coworkers have experimentally studied adsorption of beryllium on W{110} [14] and W{211} [15] surfaces. In these experiments, evaporated beryllium was deposited normal to the tungsten surface, at room temperature, and at a rate between 7×10^{11} and 4×10^{11} atoms/cm^2-s, to form 1-4 monolayer (ML) thick film of beryllium on W{110} substrate surface. Then the Be-W system was heated by ramping up the temperature at a rate of 3 or 15 K/s. This study reported that the adsorption of beryllium on the W{110} surface is dependent on the tungsten surface temperature and the surface coverage. For example, above 880 K and surface coverage of 0.64 ML (14×10^{14} atoms/cm^2) the fraction of deposited beryllium atoms adsorbed on the surface decreases rapidly while at a lower temperature all the deposited atoms get adsorbed. These results correlated with the binding energy calculated from temperature programmed desorption measurements—the binding energies of beryllium in the first layer is greater than 4.3eV, while for the second layer it drops to 3.0 eV, and above approximately 40×10^{14} atoms/cm^2 surface coverage the desorption energy is close to the sublimation energy of bulk beryllium. Additionally, authors analyzed the Work Function (WF), a surface structure sensitive metric commonly used for surface characterization, and found a complex dependence between the WF value and surface coverage. This indicated that the beryllium surface structure evolved as the coverage was increased even at sub-monolayer coverage, a result consistent with the atomistic calculations reported in [16] and discussed in section 5. Furthermore, authors gathered low-energy electron diffraction (LEED) data and inferred the arrangements of the beryllium atoms on tungsten surface with increasing surface coverage. However, since beryllium has only 4 electrons, this analysis was complex and inexact due to a low electron signal in the LEED.

When beryllium was deposited on W{211} and annealed with a ramp of 50 K/s [15], the authors concluded that the beryllium layer structure also differed based on surface coverage. In between 1- and 3.5-ML film thickness, complex structural changes occurred in the beryllium layer, depending upon the thermal history of the layer. At room temperature and below 1 ML film thickness, a beryllium monolayer with no regular structure was formed on which a second layer grew as more beryllium was deposited. Ultimately, a structure transition happened when additional beryllium was incorporated in the first layer until both the layers became high-density beryllium. For a beryllium film grown above 3.5 ML, alloying happened for both annealed and unannealed samples, mediated via formation of a dense unreacted adsorbed beryllium layer. The intermetallic formation was restricted to a few layers at the interface.

Similar film deposition experiments were performed by Sakhonenkov *et al* [17], with a very different outcome. These new experiments found that $Be_{12}W$ was formed during beryllium deposition, regardless of the thickness of the beryllium layer, and the alloy thickness increased with increasing beryllium top layer thickness. During tungsten deposition experiments, the authors found that Be_2W was formed, regardless of the thickness of the tungsten layer, and the alloy thickness did not depend on the thickness of the tungsten film; that is, there was limited alloy growth. The authors also provided detailed discussion on oxidation of these layers.

2.2. Discussion of film deposition experiments

In this section we compare the two sets of thin-film deposition experiments with very different outcomes described above: Wilter and Linsmeier's as compared to Sakhonenkov's. Table 1 compares the outcomes and conditions of these thin film deposition experiments.

Three parameters are noticeably different between these experiments. First, the substrate temperature (T) after the deposition process (annealing) was very different. Wiltner and Linsmeir annealed their samples to up to 1070 K, while Sakhonenkov *et al* only operated at room temperature. The second difference is the deposition method, and therefore most likely, the deposition rate (Γ_{depos}), although neither article provides this information. The third parameter is the impurity, in particular oxygen concentration. Sakhonenkov *et al* measured nearly fully oxidized beryllium layers after their deposition, with a contribution to the beryllium signal in the order of 60%–70%. The authors suggest that oxide formation may assist in the intermetallic formation. In contrast, Wiltner and Linsmeier report oxide contributions to the beryllium signal in the order of 10%.

Setting the oxide-mediated alloy formation hypothesis aside, and under the assumption that the deposition rate differs, we can construct a matrix with 4 quadrants for each of the target-substrate combinations. A generic example is provided in figure 3. Without sufficient detail of the experimental conditions, we may only hypothesize further on what may be driving the different outcomes. It would therefore be remarkable for a future model to reproduce these differences in alloy composition (as a function of substrate temperature and deposition rate). We would propose using this classification as part of the benchmarking process of any future material mixing model.

For this exercise, it is worth noting that the latter parameter (Γ_{depos}) may be defined by the deposition rate or the limiting element at the interface, if one of the two elements is not sufficiently available. For instance, if the beryllium deposition rate is faster than its diffusion into tungsten, a pure beryllium layer will grow, and the reaction will not be limited by the deposition rate. In contrast, if the deposition rate is slower than the diffusion rate at the interface, the material mixing will be limited by the deposition rate. This is expected in many plasma exposure experiments and likely the case in the experiments discussed in the follow two sections, where beryllium is present in impurity-level concentrations.

3. Mixed Be-W layer formation in linear plasma facilities.

3.1. Summary of results from linear plasma devices

This section reviews mixed Be-W layer growth in linear plasma devices, and specifically PISCES [8, 18]. Experiments reported by Doerner *et al* [8] used the UC-San Diego PISCES Laboratory to expose tungsten surfaces to a deuterium plasma with small (0.1%) beryllium impurity concentrations, with the goal of investigating Be-W mixed-material formation and their properties. The authors observed beryllium accumulation on the tungsten surface as well as melting of the tungsten crucible that held the hot beryllium. The

Table 1. Comparison of film-deposition conditions and results for experiments performed by Wiltner and Linsmeier [2, 10–12] (left), and Sakhonenkov [17] (right).

	Wiltner–Linsmeier	Sakhonenkov
Be → W	• Be_2W alloy formed • Limited alloy growth: restricted to the film − substrate interface • Residual Be layer of 1.2 − 1.6 nm • During annealing, Be evaporates before it reacts with W	• $Be_{12}W$ alloy formed • Alloy layer thickness increased with increasing Be top layer thickness
W → Be	• $Be_{12}W$ alloy formed • Alloy formed within the entire diffusion depth, only after annealing at $T > 1000$ K	• Be_2W alloy formed • Limited alloy growth: alloy thickness independent of the W film thickness
Experimental details	*Temperature*: • Room temperature, with annealing in steps of 100 K up to 1070 K •For XRD: Be deposited on W (∼50 nm) and annealed up to 970 K for 90 min *Method*: • Evaporated Be → polycrystalline W • Magnetron sputter 200 nm W → polycrystalline Be	*Temperature*: •Room temperature, no annealing *Method*: • Magnetron sputtering • Si substrate (100) w/roughness < 0.2 nm; then base (W or Be) 40 nm • Deposited Be layer of 0.54 nm • Deposited W layer of 0.62.8 nm

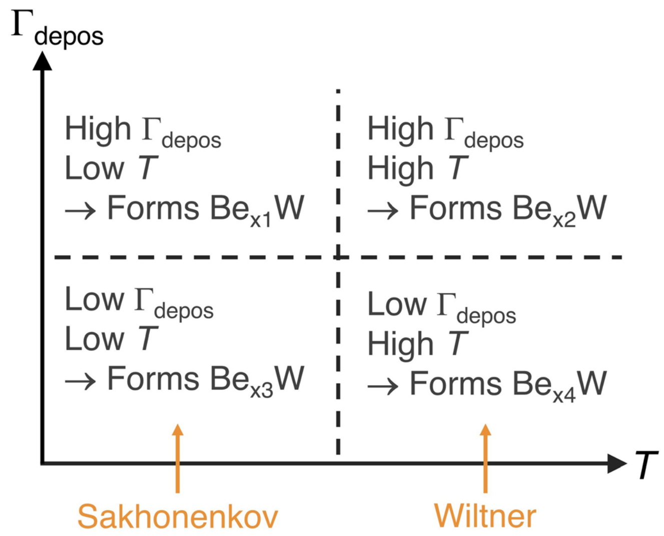

Figure 3. A generic example of a 4-quadrant matrix that could be constructed to explain the different results reported by Sahkonenkov [17] and Wiltner-Linsmeier [2, 10–12].

authors concluded that during the beryllium-seeded deuterium plasma exposure of tungsten, $Be_{12}W$ alloy begins to form at around 750 °C and $Be_{22}W$ at around 980 °C. The authors state, based on a paper by Vasina *et al* [19], that 'the Be-W reaction rate is kinetics controlled, rather than diffusion controlled, and therefore the interaction zone propagates as a wave front through the material'. While the authors do not define what is meant by kinetics controlled, we interpret this to refer to a system in which either diffusion or reaction kinetics limits the rate of formation. These mechanisms are discussed in greater detail in sections 5 and 6, although no atomistic modeling of reaction-limited kinetics is yet available. The paper also provides an estimated growth rate of the Be-W layer under plasma exposure, which is compared to values in the literature [19].

Baldwin *et al* [18] conducted collaborative experiments of beryllium-seeded D_2 plasma exposure of tungsten targets at the PISCES-B divertor-plasma simulator in UC-San Diego, which were compared with vacuum deposition experiments at Sandia National Laboratory (SNL) in Livermore, CA. The authors conclude that the efficiency of surface alloying depends on the availability of deposited beryllium, with an optimal $Be_{12}W$ alloy composition forming when beryllium is sufficiently available. During the plasma exposure at PISCES-B, the beryllium availability can be reduced by erosion and evaporation. These conclusions are based on the following observations: at a surface temperature of 1070 K, and with no target biasing (ion impact energies, $E_{in} \sim 10$ eV), a $\sim 0.3 \mu$m thick layer of $Be_{12}W$ formed. The authors attribute this finding to the high beryllium availability on the surface, due to conditions of little erosion ($E_{in} \sim 10$ eV) and little thermal evaporation ($T = 1070$ K). At similar conditions, but with a biased tungsten target ($E_{in} \sim 60$ eV), $\sim 0.3\ \mu$m nucleation zones of composition close to $Be_{12}W$ are found, distributed over a tungsten rich surface. The authors attribute the reduction in mixed-material layer formation to beryllium re-erosion. At a higher surface temperature (1150 K) and no target biasing, a $\sim 1 \mu$m thick $Be_{12}W$ alloy layer was found, which is much thinner than what would be expected based on the deposited beryllium fluence, due to beryllium evaporation. Under the same conditions but at an even higher temperature (1320 K), the authors find that the evaporative flux of beryllium at 1320 K is significantly higher than the inbound flux of beryllium during plasma exposure. These conditions lead to little evidence for any beryllium below the surface, as evaporation hindered the Be-W interaction. The resulting mixed surface has a composition close to 50:50 of Be:W, although the mixed layer thickness was not reported. In experiments with additional target biasing ($E_{in} \sim 60$ eV) and thus beryllium re-erosion, the authors find $Be_{12}W$ surface nucleation over an almost identical 50:50 of Be:W surface.

The vacuum-deposition experiments reported in the same paper [18] provide time-resolved information on the thickness of the mixed layer growth. The authors conclude that the structure of the resulting layers was similar to that observed in PISCES. At 1023 K and 1123 K, they observe net beryllium on the surface (total beryllium coverage) and a reacted layer between the beryllium and the tungsten. At 1123 K, the authors observed a uniform reacted layer approximately 1μm thick of $Be_{12}W$, with a small amount of beryllium (3.5 at.%) in the tungsten below the layer, consistent with the solubility limit. At higher temperatures (1223 K) only partial beryllium coverage is observed, with an alloy layer composition close to $Be_{50}W_{50}$. Results from the linear device plasma exposures and beryllium vacuum-deposition experiments are summarized in table 2. The original article also shows the structures of the samples exposed in PISCES (figure 1 in [18]).

Table 2. A summary of the conditions (facility, surface temperature and ion impact energy), and resulting surfaces (mixed-material thickness, beryllium coverage, and mixed-layer composition) for experiments performed in the PISCES linear plasma device at UCSD and vacuum-deposition facility in SNL.

Facility	Surface temp. (K)	Ion impact energy (eV)	Mixed-layer thickness (μm)	Be coverage	Mixed-layer composition
PISCES	1070	10	0.3	Total	$Be_{12}W$
PISCES	1070	60	0.3	Partial	$Be_{12}W$ nucleation zones in $Be_{30}W_{70}$
PISCES	1150	10	1	Partial	$Be_{12}W$
PISCES	1320	10	—	Partial	$Be_{42}W_{58}$
PISCES	1320	60	—	Partial	$Be_{48}W_{52}$ nucleation zones in $\sim Be_{12}W$
SNL	1023	<1	0.1-0.2	Total	$Be_{12}W$
SNL	1123	<1	11.5	Total	$Be_{12}W$
SNL	1223	<1	—	Partial	$Be_{50}W_{50}$

The paper also presents a particle balance model to predict which conditions (e.g. beryllium fraction in the plasma) would lead to beryllium deposition (Be in > Be out) and thus Be-W alloy formation. Further, the authors derive Be-W inter-diffusion coefficients of 4.3×10^{-15} cm^2 s^{-1} at 1023 K and 5.8×10^{-13} cm^2 s^{-1} at 1123 K [18]. In addition to the conclusions reported by the authors, we further observe from their results that the floating bias cases ($E_{\rm in} \sim 10$ eV) lead to uniform layers (figures 1(a), (c), and (d) of [18]); while biasing ($E_{\rm in} \sim 60$ eV) is correlated with the formation of beryllium-rich islands on surface, with otherwise low beryllium content (figures 1(b) and (e) of [18]).

3.2. Discussion of experiments in linear plasma devices.

Baldwin *et al* claim that evaporation leads to loss of beryllium when the surface temperature increases ($\geqslant$1150 K), although this does not appear consistent with recent atomistic modeling. These atomistic calculations involved DFT, molecular statics (MS) and molecular dynamics (MD) based on semi-empirical potentials [3, 20–22], and indicate that the surface binding energies for beryllium on beryllium or on Be-W intermetallics are in excess of 3 eV, which make evaporation rates seemingly too low at temperatures below 1300 K. Therefore, we conclude that other beryllium removal mechanisms must be at play, such as thermally enhanced sputtering or physically assisted chemical sputtering, although neither of these two mechanisms would occur during thermal deposition experiments.

The hypothesis of additional beryllium removal mechanisms is consistent with other experimental literature [23–25]. Doerner *et al* [23, 24] and Schmid *et al* [25] experimentally measured erosion rates of metal surfaces exposed to energetic particle bombardment at an elevated temperature to research thermally-assisted or thermally-enhanced surface erosion [23–25]. These high-flux deuterium and helium plasma exposures were performed at the PISCES-B facility, and the authors developed a model to predict thermally enhanced beryllium erosion rates, which was parametrized by atomistic simulations. All three studies concluded that, in addition to physical sputtering (which is temperature independent) and sublimation (which is flux independent and only relevant at higher surface temperatures), additional mechanism(s) must be responsible for increasing the erosion rate of beryllium. This additional mechanism might enable sublimation at lower temperatures than expected from evaporation, and thus explains the higher-than-expected beryllium erosion observed at high (>1000 K) temperatures. Doerner *et al* [23, 24] hypothesize that this mechanism is adatom formation by the incoming energetic ions, whereas Schmid *et al* [25] suggest 'the formation of weakly bonded surface atoms due to inclusion of the implanted species below the surface' (in their case, helium).

We believe that a similar mechanism might also have been at play in the PISCES experiments of Be-W mixing [18], although the specifics may differ. First, the substrate composition differs: in the material mixing experiments [18], the substrate is initially tungsten and later mixed Be-W, whereas erosion experiments [23–25] used a beryllium substrate. Second, beryllium is deposited on tungsten (and thus starts the process as an adatom) in the material mixing experiments, while beryllium is the substrate matrix in the erosion experiments. Third, the ions come at lower incidence energies ($E_{\rm in} \sim 10$ eV) in most of the material mixing experiments, compared with the erosion experiments ($E_{\rm in} \sim 50$ eV). Finally, in comparison to Schmid *et al* [25], the plasma is mainly composed of deuterium in material mixing experiments, instead of helium. This is an important difference as, unlike helium, deuterium binds to beryllium and may form molecules that can chemically erode (within energy and temperature range of material mixing experiments, 10–60 eV and 300–1300 K, respectively). While this molecular formation may lower the surface binding energy, this supposition involves a different mechanism

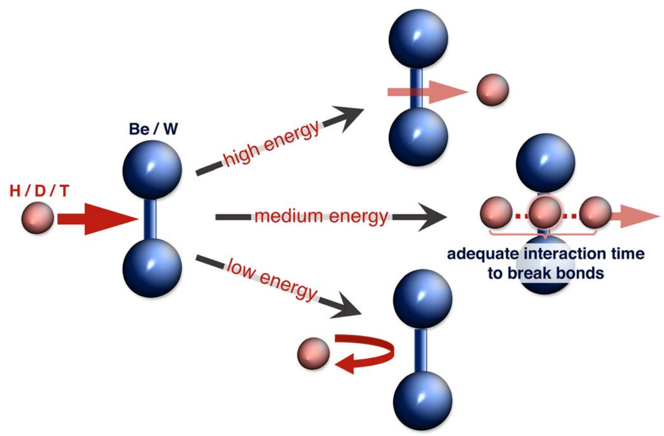

Figure 4. Schematic figure of swift chemical sputtering, depicting a hydrogenic ion that impacts on beryllium dimer, showing: the ion bouncing back when the impact energy is too low to interact with the dimer bond; the ion is breaking the dimer bond when the impact energy is within the medium range; and, the ion moving through the bond without interacting when the impact energy is high and thus time spent in the bonding region is too short to interact. The figure is adapted from figure 2 of [27] to show the materials of interest, i.e. Be and W. Reuse permitted by Elsevier. Copyright (2002) Elsevier Science B.V.

than that suggested by Schmid or Doerner (e.g. adatom formation of sub-surface gas accumulation). Molecular erosion of beryllium is further discussed later in this section.

It is worth noting that, beyond the molecular dynamics simulations performed by Schmid *et al* to parametrize their model, fundamental (e.g. atomistic) work is lacking in these papers to explore the origin of the sublimation assisting mechanism. Therefore, in our view, the mechanisms proposed by Doerner and Schmid remain an unproven hypothesis. Their model output matches the experimentally measured beryllium erosion, with very few free parameters, if any, but only for these very specific conditions. This approach of model validation resembles that of Baldwin *et al*, where evaporation explained the beryllium outflux observed in their experiments, yet recent atomistic work suggests that beryllium sublimation from mixed Be-W surfaces is very unlikely at surface temperatures of 1000–1300 K.

As mentioned above, molecular erosion of beryllium may also be at play in these experiments. Swift chemical sputtering (SCS, also known as chemically assisted physical sputtering, CAPS) [5, 26–28] is another mechanism that has been shown to enhance beryllium erosion. In this process, an energetic ion has an energy interval in which it possesses sufficient energy to break a surface bond and remains in the vicinity of the surface for sufficient time to create a new chemical bond with one or more of the near surface atoms, as shown schematically in figure 4. Therefore, both ion kinetic energy (thus, ion incidence energy, E_{in}) and target-ion bond interactions (thus, surface temperature) are at play in CSC. The ion incidence energy window where SCS may be relevant depends on the strength of ion-target bonds and ion-target mass ratio. For instance, for a beryllium dimer (bonding energy ~1 eV), the energy window is $E_{\text{in}} \sim 3 - 36$ eV. The behavior is more complex for dimers of mixed materials, both due to the mass difference and the energetic asymmetry introduced by the different bonding interactions. SCS leads to the formation of molecules. Specifically in the case of deuterium incident onto beryllium, beryllium deuteride molecules BeD, BeD_2, and likely BeD_3 form and then are subsequently released from the surface. Safi *et al* simulated low-energy deuterium irradiation of beryllium using molecular dynamics simulations to calculate beryllium sputtering yields as a function of the surface temperature, finding that erosion increased dramatically at temperatures greater than 600 K. The authors attribute this enhanced erosion to easier bond breaking due to increased atomic vibrations. In their simulations, most of the eroded beryllium was released as BeD and BeD_2, both of which are stable molecules. BeD_3 is also formed by SCS; however, it is metastable and breaks into BeD+D_2 after being released from the surface [29] and therefore it may not be observed experimentally.

Finally, there are other considerations to keep in mind when determining the process(es) that leads to thermally enhanced erosion of beryllium. As reported in [30], S. Lisgo *et al* highlight that much higher beryllium sputtering rates are found for redeposited material than the original substrate. Further, Doerner *et al* reported a lower sticking coefficient of re-deposited beryllium than is expected from the literature. These two mechanisms, in addition to highly defected surface layers, would be expected to enable beryllium erosion with kinetic energy and/or temperature lower than expected.

4. Confinement devices: JET

Be-W mixed material layer formation has also been observed in confinement devices, as shown previously in figure 1. This data is much more limited than for non-confinement facilities, as the two elements are currently only present in the JET tokamak. Each of the stable Be-W intermetallic compounds have been found in different areas of JET since its change to an ITER-like wall. Analysis of the divertor after the 2011-2012 campaign found Be-W compounds on tile 1/8 (upper area of the inner divertor) and showed formation of mixed Be-W material layer on sample 6/6 (outer divertor corner), although the authors do not specify the layer composition [31, 32].

Additionally, Be-W intermetallic compounds have been found on the sides of the castellated beryllium limiters, which are considered a material deposition zone. Rubel *et al* found all three stable alloy compositions (Be_2W, $Be_{12}W$, $Be_{22}W$) during the 2011-2012 and 2013-2014 campaigns [33]. Litaudon *et al* also reported the presence of Be-W mixed intermetallic compounds in limiter tiles during the 2014-2016 campaign, although the authors did not specify the composition of these layers [34]. Finally, Jepu *et al* found $Be_{22}W$ in the beryllium waterfall structure formed in the dump plate tile 8 (at the top of the machine) during the ILW-2 (2013-2014) campaign [35].

5. Modeling Be-W interactions

Based on the phase diagram described in the Introduction, and under the assumption that the beryllium deposited on the tungsten surface would be relatively dilute, then the tungsten-rich intermetallic Be_2W phase is expected to form due the to surface alloying reaction. However, both Be_2W and $Be_{12}W$ have been observed to form experimentally [2, 10–13], which indicates that the growth of the intermetallic beryllium phase is kinetically controlled. Therefore, the mixed layer growth is strongly dependent on the elemental kinetic steps such as adsorption of the implanted/deposited metal on the surface and diffusion of the implanted/deposited metal from surface into the bulk and in the bulk. Furthermore, the plasma environment would drive the loss of metal from the surface and hence influence the surface intermetallic composition. Insights into these kinetic steps from computational simulations found in the literature is the focus of the remainder of this section.

There are a limited number of first principle based atomistic calculations available in the literature [3, 16, 22, 36–39] to understand the Be-W thermodynamics and surface interactions. There are also a number of molecular statics and dynamics simulations available in the literature [16, 21, 22, 40–46] to understand the kinetics of beryllium-tungsten intermetallic layer formation and growth. Chen's latest work [47], as well as Bjorkas' and Lasa's simulations focused on erosion and mixing through energetic ion implantation: irradiation of tungsten by beryllium, of mixed Be-W by deuterium, and of tungsten by D-Be. While their work fits within the general scope of this paper, it goes beyond the topic explored in this section, which focuses on more static calculations in order to understand the role of adsorption and diffusion in Be-W mixing and intermallic growth.

Allouche and coworkers [36–38] used DFT to estimate beryllium adsorption energy on the tungsten surface and the barrier for metal beryllium adatom to enter from surface into bulk tungsten, and vice versa. They found that tungsten adsorption on the basal (0001) beryllium surface is a barrier free process with the stable adsorption site in a potential well of -4.2 eV [36, 38]. In the case of beryllium adsorption on the W(100) surface, the process is also barrier free into a potential well of a depth of -2.3 eV at 1.72 Å above the surface in a bridge position between two tungsten atoms. For the W(111) surface, it is also barrier free with a double well minima where one minimum of -1.8 eV is for beryllium atom adsorbed at 1.5 Å above the tungsten surface and the other minimum is of -2.6 eV for beryllium in the surface layer. The barrier between these two minima is due to the reorganization of the surface around the arriving beryllium and involves a 0.4 eV barrier for migration from the first to the second well [37, 38]. Additionally, Allouche and coworkers have reported that sequential addition of beryllium leads to the adsorption energy reaching a limit of -4.0 eV, close to the cohesive energy of metallic beryllium (3.7 eV) [37]. This result is consistent with DFT calculations by Yang [39]. Due to the small supercell size, the study by Allouche *et al* could not provide additional information on the structure of clusters formed by adsorption of multiple beryllium atoms and subsequent growth of the beryllium layer on top of tungsten.

To that end, Hatton and coworkers have used DFT computations to study the structures of the beryllium layer on W(110) and W(211) surfaces as a function of surface coverage [16]. Similar motifs of beryllium surface structures were found on both surfaces. At very low surface coverage (14.3×10^{14} atoms/cm^2), beryllium forms isolated clusters or islands where beryllium occupies the tungsten lattice site of the next layer. At low density uniform coverage (16.7×10^{14} atoms/cm^2), beryllium forms open hexagonal patterns. At intermediate coverage (24.8×10^{14} atoms/cm^2), when the beryllium layer thickness is more than an ML, the first layer is a low density region with uniform coverage, but the next incomplete layer contains a high density region where beryllium occupies a densely packed hexagonal lattice structure. These surface structures were verified through calculation of the WF and compared to experimental calculations provided by Schlenk, Chrzanowski and coworkers [14, 15]. There was a strong agreement between the WF values indicating that the DFT analysis generated experimentally valid structures. While there were some discrepancies between the physical beryllium surface structures from DFT versus those inferred experimentally, the experimental inference was based on LEED pattern analysis which was difficult to verify since beryllium has only 4 electrons, too low to produce a sharp pattern as mentioned in [16], possibly leading to misinterpretations of the LEED pattern and therefore differences in the inferred beryllium surface structure. Furthermore, Hatton and co-workers used the DFT structures to produce a simulated LEED pattern which visually matched well with experimental images further reinforcing the validity of the DFT structures. With increasing beryllium layer thickness beyond a few 3-4 MLs, subsequent layers assume metallic hcp beryllium structures, a result which is consistent with first principle based calculations [16] and experiments [14, 15].

Surface relaxation leads to a first interlayer distance of 1.830 Å for the Be(0001) surface, as opposed to 1.752 Å in the bulk. This is an insignificant change compared with certain surfaces like W(100), which undergoes a more extensive relaxation or surface reconstruction [36–38]. It is further reported that, an adsorbed tungsten atom has to cross a barrier of 1.6–1.8 eV to enter into the host beryllium layer and must first cross two surface beryllium layers in order to penetrate into the bulk, where the minimum interaction energy with the host is -4.5 eV, comparable to the adsorption energy. In contrast, in case of an adsorbed beryllium atom on W(100) and W(111) surfaces, the barriers to penetrate into the subsurface position are about 3.6 eV and 5.2 eV, respectively, due to the surface reconstruction [36–38]. However, in both cases, the interaction energy minima are too shallow and the W(5d)Be(2p) interaction is too weak to achieve an energetically stable structure, relative to the surface adsorbed state or the non-interactive state—a pure tungsten surface and the beryllium atom far from it. As a consequence, it is energetically unfavorable for beryllium atoms to diffuse inside the bulk tungsten. These results are consistent with DFT calculations by Hatton *et al* [21] and MD simulations using spectral neighbor analysis potentials (SNAP) [21]. Energy barriers calculated by Allouche and coworkers for diffusion of beryllium or tungsten in the bulk should be considered with a strong caveat: no zero-point energy correction was performed (although in fairness, it might not have a significant effect on the results), and the supercells used in these calculations are very small (Be(0001): 44 Be atoms in 5 layers; W(100): 29 W atoms in 7 layers; W(111) 36 W atoms in 9 layers) [37]. The adsorption and near-surface diffusional energy barriers for Be-W system calculated using analytical bond-order potential (ABOP) agree qualitatively with *ab initio* calculations [40]. Using the SNAP potential, Hatton and coworkers have calculated the diffusional energy barrier for beryllium in bulk intermetallics to be ∼0.3 eV [21]. However, the diffusional pathways for the beryllium interstitial are highly anisotropic [21].

Chen and coworkers have also used DFT to extend the energy calculations of tungsten and beryllium adsorption on a wider range of surface orientations. In particular, they examined Be(0001), Be$(11\bar{2}0)$, Be$(11\bar{2}1)$, W(001), W(110), W(111), $Be_2W(001)$, $Be_2W(110)$, $Be_2W(111)$, $Be_{12}W(001)$, $Be_{12}W(110)$, and $Be_{12}W(111)$ orientations [22]. The beryllium adsorption energy on different beryllium surfaces is within a range of 2–2.7 eV whereas on intermetallic surfaces it varies between 3 and 4.3 eV (adsorption energy calculated as the difference between the formation energies of a surface-adsorbed beryllium atom and a hexagonal closed packed beryllium atom). However, a beryllium adatom is weakly bound to tungsten surfaces with an adsorption energy between 0.4 and 1.38 eV, a much smaller value than that reported by Allouche and coworkers [36]. The difference is attributed to larger supercell size facilitating surface relaxation in case of Chen and coworkers [22]. However, for tungsten on beryllium surfaces the calculated adsorption energy is consistent between the two studies due to the smaller surface relaxation, and it varies between 3.8 to 5.7eV depending on beryllium surface orientation. With increasing tungsten atom concentration at the intermetallic surface, the adsorption energy of tungsten increases from 4.8 to 9.7 eV, whereas on a pure tungsten surface the range is between 7.6 to 8.9 eV [22].

As indicated earlier in section 2.1, the DFT calculated surface binding energies [22] are too high to allow significant thermally activated desorption of beryllium at or below 1300 K; namely, a minimum value of 6.81eV for $Be_{12}W(001)$ and a maximum value of 10.27 eV for W(110). The Be-W dimer binding energy is predicted to be 1.82 eV and the desorption energy of beryllium from the W(110) surface is 3.5 eV for 0.6×10^{14} atoms/cm^2 surface coverage and ∼4 eV for any other surface coverage up to $\sim 14.2 \times 10^{14}$ atoms/cm^2 [39], again too high for beryllium to sublimate (thermally evaporate) at or below 1300 K. Schlenk *et al* [14] have reported that in case of thin film experiment, the rate of beryllium evaporation is a function of surface coverage, with desorption energy varying between 4-4.8eV for a monolayer thick film; for the second layer it drops to 3 eV. In their calculation, Yang *et al* [39] used a beryllium surface layer motif where beryllium atoms sit in place of tungsten atoms in the next layer, which corresponds to low surface coverage [16]. These calculations need to be extended for other motifs reported by Hatton *et al* [16] to understand the dependence of desorption energy on surface coverage. Furthermore, Chen *et al* [22] reported the adatom binding energy to complete a perfect step is too high. However, in practice, step edges are partially complete and the adatom binding energy for such a step should be lower than a complete step and hence desorption from such a step should be relatively favorable. Additional atomistic calculations are needed to quantify the adatom binding energy at the partially complete stable edges and at the kink to validate this hypothesis. Therefore, collective mechanisms associated with sub-threshold physical sputtering, such as chemically assisted sputtering of beryllium by deuterium [5, 28] and thermally assisted physical sputtering (discussed in section 3.2) [23–25] are the most likely mass loss mechanisms under these experimental conditions (Note: Experimentally measured sputtering threshold of beryllium by D^+ is ~10eV [48], in agreement with the computational work referenced in section 3.2).

In summary, beryllium atoms deposited on the tungsten surface get strongly adsorbed and after the first couple of deposited layers beryllium atoms start forming hcp metallic beryllium layers. There is a significant energy barrier for beryllium atoms adsorbed on the tungsten surface to move past the surface layer and get mixed with tungsten. In this case, two reported mechanisms of beryllium atom diffusion from the surface/interface to inside the host tungsten layer are: (i) vacancy mediated diffusion and (ii) ring diffusion (exchange of tungsten and beryllium atoms), provided beryllium deposition is slow enough to not form more stable beryllium clusters, beryllium stays as surface adatoms. In the case of beryllium film deposition on tungsten at low temperature followed by annealing at high temperature (as in the experiments by Wiltner and Linsmeier, discussed in section 2.1), the only plausible mixing mechanism is vacancy mediated diffusion for which no computation study is currently available in the literature. In contrast, for high energy beryllium implantation in tungsten, the near-surface energy barrier for beryllium diffusion does not have any influence on the mixing process. Once enough beryllium is implanted inside the tungsten matrix and the local beryllium concentration relative to tungsten is high enough, Be-W intermetallics start forming. Additionally, due to difference in cohesive energies and masses between beryllium and tungsten, the former will be preferentially sputtered. In case of tungsten deposited on beryllium, tungsten can easily migrate into the host atoms due to absence of any near surface barrier and tungsten inside the beryllium host is energetically favorable. Therefore, in both caseshigh energy implantation and low energy depositiontungsten diffuses inside beryllium and forms a uniformly mixed layer of Be-W which then converts to a stable intermetallic structure.

6. Discussion of experimental results based on computational understanding of Be-W interactions

In light of the atomistic modeling results discussed above, the results of film deposition experiments [2, 10–12, 14, 15] can be interpreted as follows. When beryllium is deposited on a tungsten substrate, the first two monolayers are strongly bound to the surface, as reflected by a strong adsorption energy well with values between −2.3 and −2.6 eV, varying depending on the tungsten surface orientation [36–38], and a high desorption energy barrier of 4 eV [39]. Additionally, the high energy barrier of 1.5−1.8eV [36, 37] for beryllium to diffuse past/through the top two surface layers of tungsten inhibits beryllium diffusion from the tungsten surface in towards the bulk (noting that calculations using semi-empirical interatomic potentials report an even higher barrier [40]). As a result, the Be-W intermixed layer is restricted to the interface region, which is consistent with the observations reported for thermal deposition experiments in [2, 10–12, 14, 15].

MD simulations of Hatton and co-workers [21] show that in the absence of any near surface defect, the beryllium and tungsten layers do not intermix within molecular dynamics time-scales (about 10 ns). However, in the presence of a tungsten vacancy or beryllium interstitial, a defect-mediated diffusion mechanism facilitates the intermixing of beryllium and tungsten layers, and this provides an indication of a prerequisite for Be-W intermetallics formation. That is, any surface defect will facilitate intermixing once a stable Be/W bilayer is formed. During annealing experiments, an increase in temperature is likely to drive both motion of any induced vacancies as well as to increase the equilibrium vacancy contraction. This may be a plausible factor behind the increase in (vacancy-mediated) beryllium diffusion and intermixing of Be-W at elevated temperatures. To date, all of the atomistic studies available in the literature are focused on diffusion of beryllium as an interstitial; this suggests a need for an in-depth atomistic study on the vacancy-mediated diffusion of beryllium in tungsten to understand and validate this hypothesis.

In the case of tungsten deposition on a beryllium substrate, tungsten adatoms have to overcome an energy barrier of 1.6–1.8 eV (only feasible at elevated temperature of ~1000 K, however relatively low in comparison to diffusion of beryllium into tungsten) to migrate from the surface to the bulk of beryllium [37, 38]. Additionally, unlike the inclusion of free beryllium into bulk tungsten, inclusion of free tungsten into beryllium is an endothermic process [36, 38], which favors mixing of tungsten into beryllium and formation of a beryllium-rich, thick mixed-layer. During tungsten deposition on a beryllium surface, it is natural to form the beryllium-rich $Be_{12}W$ phase before the Be_2W phase. Therefore, even if the latter is more thermodynamically stable, and for a sufficiently strong local minimum between these phases, the system may not be able to transition to Be_2W and thus a $Be_{12}W$ mixed-material layer would form.

We do not present any analysis of Sakhonenkov *et al* [17], as the Be:W stoichiometries found in their film deposition experiments may be an anomaly due to the presence of high concentration of oxygen in the system.

The authors discussed a probable reaction mechanism of Be-W intermetallics formation via oxidation of beryllium and tungsten layers, followed by a reaction between beryllium and tungsten oxides. At present we do not have all the necessary atomistic data available in literature to evaluate this hypothesis.

Further, in the experiments by Baldwin and Doerner [8, 18], energetic beryllium-containing plasma of ~10 or 60 eV is implanted in tungsten. Since the beryllium atoms in these experiments have sufficient energy to overcome the near-surface diffusional barrier of 1.5–1.8 eV [37, 38], intermixing of beryllium and tungsten is feasible and hence formation of intermetallic compounds is too. For the floating bias cases (~10 eV), beryllium atoms have just enough energy to move past the near surface region and are then driven by Fickian diffusion, since the diffusional energy barrier is low ~0.3 eV. Therefore, a propagating reaction front can explain the observed growth of the thick intermetallics layers. For the case with surface biasing (~60 eV), the intermetallic formation is a combined effect of implantation profile and diffusion-driven local reaction kinetics, which has a strong dependence on the local beryllium contraction. This may explain the intermetallic nucleation zones observed in otherwise W-rich layers. Further, at this implantation energy, it is expected that a combination of near surface vacancy and adatom formation (sub-threshold sputtering reactions) can also locally increase the vacancy concentrations to further promote inter-diffusion, similar to the diffusion of neon in tungsten as discussed in [49]. MD simulations using SNAP potentials confirm surface adatom and near-surface vacancy formation during low-energy beryllium implantation in tungsten [20]. This complex dynamical phenomenon is beyond the scope of this discussion. An atomistically informed mesoscopic/continuum model is best suited to understand and explore the intermetallics formation formation in linear plasma experiments.

There are additional considerations we would like to highlight when addressing the formation of Be_2W versus $Be_{12}W$. PISCES experiments as well as beryllium film deposition experiments by Sahkonenkov *et al*. show preferential formation of $Be_{12}W$, whereas both DFT and MS calculations (and experiments by Wiltner and Linsmeier [2, 10–13]) show that Be_2W is most stable. However, it is worth noting that both $Be_{12}W$ and Be_2W have been observed in MD simulations of beryllium implantation in tungsten [46]. We may reconcile these differences considering that while Be_2W is most stable at 0 K (in the atomistic calculations), it may not be the most stable structure at higher temperatures ($T > 1000$ K). Furthermore, as these are non-equilibrium processes, it is always possible that $Be_{12}W$ is metastable but is preferentially formed under these conditions, as can often happen during film growth. This hypothesis should be tested with additional atomistic calculations. Finally, it is worth noting once again that while $Be_{12}W$ might form when sufficient beryllium is made available to the tungsten or mixed-material matrix [8, 18], this availability may be reduced by several factors: insufficient deposition or a lower-than-expected sticking coefficient, as reported by Doerner *et al* (IAEA report above); and insufficient diffusion due to low temperature, low beryllium coverage at high temperatures due to the low beryllium binding energy to a pure tungsten surface [22], too short time (affecting simulations), or an extra barrier at the Be-W interface present in film deposition experiments, compared with implantation that happens during plasma experiments and simulations.

7. Summary and future needs

We have reviewed the existing literature of computational and experimental studies of Be-W material mixing. Interpretation of the experiments using fundamental insights from atomistic modeling of the system allows for an assessment of the Be-W growth kinetics. We conclude that the following kinetic steps drive the material mixing: adsorption of the implanted/deposited ion on the metal surface; diffusion of the implanted/deposited ion from surface into the bulk, which is accelerated by defects; and loss of deposited material through erosion. Adsorption dominates material mixing in thin-film deposition experiments: during beryllium deposition on tungsten, the first two monolayers are strongly bound to the surface by an energy well of −2.3 to −2.6 eV and a high desorption energy barrier of ~4 eV. Additionally, the high energy barrier of 1.5–1.8 eV for a thermally deposited beryllium atom of energy less than 1 eV to diffuse past the top two layers of tungsten prevents beryllium migration towards the tungsten bulk. As a result, the mixing of Be-W is restricted to the interface region. In contrast, during deposition of tungsten on a beryllium surface, the energy barrier for migration of tungsten towards the beryllium bulk is relatively low (1.6–1.8 eV). Further, inclusion of tungsten into the beryllium matrix is an endothermic process, which promotes mixing of the two materials and formation of a beryllium-rich, $Be_{12}W$ layer. In linear plasma experiments, plasma ions have sufficient energy to overcome the near-surface diffusional barrier. Therefore, adsorption plays a smaller role and diffusion dominates material mixing. A propagating reaction front can explain the observed growth of the thick intermetallic layers.

However, the system is not yet fully understood, especially in the more dynamic (e.g. plasma exposure) environment. For instance, to date, all of the atomistic studies available in the literature are focused on diffusion of beryllium as an interstitial. However, vacancy mediated diffusion of beryllium into the tungsten matrix has been shown to promote material mixing. This gap calls for an in-depth atomistic study on this mechanism to understand and validate the hypothesis. Additional atomistic simulations are also needed to fully evaluate the mechanism(s) that leads to thermally-enhanced sputtering of beryllium. Atomistic simulations are also required to better understand the mixed material formation that is governed by reaction-limited kinetics. Furthermore, at present we do not have all the necessary atomistic data available in the literature to evaluate the contribution of impurities, most notably the hypothesis of oxide-mediated Be-W alloy formation. In addition to presenting an additional path for Be-W alloy formation, understanding this mechanism is necessary to resolve the discrepancies between thin-film deposition experiments. Finally, meso- and continuum-scale modeling is needed for predicting the Be-W phase-space and layer thickness.

Acknowledgments

Authors acknowledge support by the U.S. Department of Energy, Office of Fusion Energy Sciences (OFES) and Office of Advanced Scientific Computing Research through the Scientific Discovery through Advanced Computing (SciDAC) project on Plasma-Surface Interactions through UT-Battelle Subcontract No. 4000159718, and partially supported by OFES Award No. DE-SC0006661.

This article has been authored by an employee of National Technology & Engineering Solutions of Sandia, LLC under Contract No. DE-NA0003525 with the U.S. Department of Energy (DOE). The employee owns all right, title and interest in and to the article and is solely responsible for its contents. The United States Government retains and the publisher, by accepting the article for publication, acknowledges that the United States Government retains a non-exclusive, paid-up, irrevocable, world-wide license to publish or reproduce the published form of this article or allow others to do so, for United States Government purposes. The DOE will provide public access to these results of federally sponsored research in accordance with the DOE Public Access Plan.

This paper describes objective technical results and analysis. Any subjective views or opinions that might be expressed in the paper do not necessarily represent the views of the U.S. Department of Energy or the United States Government. This article was partly authored by employees of Los Alamos National Laboratory which is operated by Triad National Security, LLC, for the National Nuclear Security Administration of the U.S. Department of Energy (Contract No. 89 233 218CNA000001).

Data availability statement

No new data were created or analysed in this study.

ORCID iDs

Ane Lasa https://orcid.org/0000-0002-6435-1884
Dwaipayan Dasgupta https://orcid.org/0000-0001-9405-922X
Matthew J Baldwin https://orcid.org/0000-0001-6335-2255
Mary Alice Cusentino https://orcid.org/0000-0001-9505-6442
Peter Hatton https://orcid.org/0000-0002-2914-2200
Danny Perez https://orcid.org/0000-0003-3028-5249
Blas P Uberuaga https://orcid.org/0000-0001-6934-6219
Li Yang https://orcid.org/0000-0003-2216-6071
Brian D Wirth https://orcid.org/0000-0002-0395-0285

References

[1] Mayer M *et al* 2016 Erosion and deposition in the JET divertor during the first ILW campaign *Phys. Scr.* **2016** 014051 (JET Contributors)
[2] Wiltner A and Linsmeier C 2006 Surface alloying of thin beryllium films on tungsten *New J. Phys.* **8** 181
[3] Gyoeroek M, Kaiser A, Sukuba I, Urban J, Hermansson K and Probst M 2016 Surface binding energies of beryllium/tungsten alloys *J. Nucl. Mater.* **472** 76–81
[4] Walsh K A 2009 *Beryllium Chemistry and Processing* (ASM International) (https://doi.org/10.31399/asm.tb.bcp.t52230093)
[5] Björkas C, Borodin D, Kirschner A, Janev R K, Nishijima D, Doerner R P and Nordlund K 2013 Multiscale modeling of bed release and transport in PISCES-B *J. Nucl. Mater.* **438** S276–9
[6] Wachowicz E and Kiejna A 2001 Bulk and surface properties of hexagonal-close-packed Be and Mg *J. Phys. Condens. Matter* **13** 10767
[7] Okamoto H and Tanner L E 1986 The Be-W (Beryllium-Tungsten) system *Bulletin of Alloy Phase Diagrams* **7** 356–8
[8] Doerner R P, Baldwin M J and Causey R A 2005 Beryllium-tungsten mixed-material interactions *J. Nucl. Mater.* **342** 63–7
[9] Takagi T 1984 Ion-surface interactions during thin film deposition *J. Vac. Sci. Technol.*A **2** 382–8
[10] Wiltner A and Linsmeier C 2005 Formation of a surface alloy in the beryllium-tungsten system *J. Nucl. Mater.* **337-339** 951–5

[11] Linsmeier C, Ertl K, Roth J, Wiltner A, Schmid K, Kost F, Bhattacharyya S R, Baldwin M J and Doerner R P 2007 Binary beryllium-tungsten mixed materials *J. Nucl. Mater.* **363-365** 1129–37
[12] Wiltner A, Kost F, Lindig S and Linsmeier C 2007 Structural investigation of the Be-W intermetallic system *Phys. Scr.* **T128** 133
[13] Linsmeier C, Reinelt M and Schmid K 2011 Surface chemistry of first wall materials - From fundamental data to modeling *J. Nucl. Mater.* **415** S212–8
[14] Schlenk W and Bauer E 1980 Beryllium films on the tungsten 110 surface *Surf. Sci.* **94** 528–46
[15] Chrzanowski E and Bauer E 1986 The adsorption of beryllium on the tungsten (211) surface *Surf. Sci.* **173** 106–27
[16] Hatton P, Perez D and Uberuaga B P 2022 Be surface structures on W(110) and W(211): a DFT study *Acta Mater.* **235** 118012
[17] Sakhonenkov S S and Filatova E O 2020 Interface formation between Be and W layers depending on its thickness and ordering *Appl. Surf. Sci.* **534** 147636
[18] Baldwin M J, Doerner R P, Nishijima D, Buchenauer D, Clift W M, Causey R A and Schmid K 2007 Be-W alloy formation in static and divertor-plasma simulator experiments *J. Nucl. Mater.* **363-365** 1179–83
[19] Vasina E A and Panov A S 1974 Reactions between tungsten and beryllium *Russian Metallurgy (Metally)* **1** 119–21
[20] Molecular dynamics simulation work on Be evaporation and molecular static calculations of binding energies. Private communication with M.A. Cusentino
[21] Molecular dynamics simulation work on mixing of Be thin film and W substrate, and molecular static calculations of Be binding energies. Private communication with P. Hatton
[22] Chen L, Sukuba I, Probst M and Kaiser A 2018 Beryllium, tungsten and their alloys Be_2W and $Be_{12}W$: Surface defect energetics from density functional theory calculations *Nuclear Materials and Energy* **16** 149–57
[23] Doerner R P, Krasheninnikov S I and Schmid K 2004 Particle-induced erosion of materials at elevated temperature *J. Appl. Phys.* **95** 4471–5
[24] Doerner R P, Baldwin M J, Krasheninnikov S I and Schmid K 2005 High temperature erosion of beryllium *J. Nucl. Mater.* **337-339** 877–81
[25] Schmid K, Baldwin M J and Doerner R P 2006 Modelling of thermally enhanced erosion of beryllium *J. Nucl. Mater.* **348** 294–301
[26] Nordlund K, Björkas C, Vörtler K, Meinander A, Lasa A, Mehine M and Krasheninnikov A V 2011 Mechanism of swift chemical sputtering: Comparison of Be/C/W dimer bond breaking *Nucl. Instrum. Methods Phys. Res.*B **269** 1257–61
[27] Krasheninnikov A V, Nordlund K, Salonen E, Keinonen J and Wu C H 2002 Sputtering of amorphous hydrogenated carbon by hyperthermal ions as studied by tight-binding molecular dynamics *Comput. Mater. Sci.* **25** 427–34
[28] Safi E, Björkas C, Lasa A, Nordlund K, Sukuba I and Probst M 2015 Atomistic simulations of the effect of reactor-relevant parameters on be sputtering *J. Nucl. Mater.* **463** 805–9
[29] Sukuba I, Kaiser A, Huber S E, Urban J and Probst M 2017 Energetics and reactivity of small beryllium deuterides *J. Mol. Model.* **23** 203
[30] Braams B J 2011 *Data Needs for Erosion and Tritium Retention in Beryllium Surfaces* International Atomic Energy Agency, Vienna, Austria Technical Report (https://osti.gov/etdeweb/biblio/21541917)
[31] Masuzaki S *et al* (JET contributors) 2017 Analyses of microstructure, composition and retention of hydrogen isotopes in divertor tiles of JET with the ITER-like wall *Phys. Scr.* **2017** 014031
[32] Oya Y *et al* 2018 Correlation of surface chemical states with hydrogen isotope retention in divertor tiles of JET with ITER-like wall *Fusion Eng. Des.* **132** 24–8
[33] Rubel M *et al* (JET Contributors) 2017 Fuel inventory and deposition in castellated structures in JET-ILW *Nucl. Fusion* **57** 066027
[34] Litaudon X and (JET Contributors) 2017 Overview of the JET results in support to ITER *Nucl. Fusion* **57** 102001
[35] Jepu I *et al* (JET Contributors) 2019 Beryllium melting and erosion on the upper dump plates in jet during three ITER-like wall campaigns *Nucl. Fusion* **59** 086009
[36] Allouche A and Linsmeier C 2008 Quantum study of tungsten interaction with beryllium (0001) *J. Phys. Conf. Ser.* **117** 012002
[37] Allouche A, Wiltner A and Linsmeier C 2009 Quantum modeling (DFT) and experimental investigation of beryllium-tungsten alloy formation *J. Phys. Condens. Matter* **21** 355011
[38] Allouche A 2009 Electronic aspects of beryllium-tungsten surface alloying, a density functional approach *Chem. Phys. Lett.* **470** 119–22
[39] DFT simulation work on Be adsorption and desorption energy. Private communication with L. Yang
[40] Björkas C, Henriksson K O E, Probst M and Nordlund K 2010 A Be-W interatomic potential *J. Phys. Condens. Matter* **22** 352206
[41] Lasa A, Heinola K and Nordlund K 2014 Atomistic simulations of Be irradiation on W: mixed layer formation and erosion *Nucl. Fusion* **54** 083001
[42] Lasa A, Heinola K and Nordlund K 2014 The effect of beryllium on deuterium implantation in tungsten by atomistic simulations *Nucl. Fusion* **54** 123021
[43] Lasa A, Schmid K and Nordlund K 2014 Modelling of W-Be mixed material sputtering under D irradiation *Phys. Scr.* **2014** 014059
[44] Wood M A, Cusentino M A, Wirth B D and Thompson A P 2019 Data-driven material models for atomistic simulation *Phys. Rev.* B **99** 184305
[45] Cusentino M A, Wood M A and Thompson A P 2020 Suppression of helium bubble nucleation in beryllium exposed tungsten surfaces *Nucl. Fusion* **60** 126018
[46] Cusentino M A, Wood M A and Thompson A P 2021 Beryllium-driven structural evolution at the divertor surface *Nucl. Fusion* **61** 046049
[47] Chen L, Kaiser A, Probst M and Shermukhamedov S 2021 Sputtering of the beryllium tungsten alloy Be_2W by deuterium atoms: molecular dynamics simulations using machine learned forces *Nucl. Fusion* **61** 016031
[48] Guseva M I, Suvorov A L, Korshunov S N and Lazarev N E 1999 Sputtering of beryllium, tungsten, tungsten oxide and mixed W-C layers by deuterium ions in the near-threshold energy range *J. Nucl. Mater.* **266-269** 222–7
[49] Backman M, Hammond K D, Sefta F and Wirth B D 2016 Atomistic simulations of tungsten surface evolution under low-energy neon implantation *Nucl. Fusion* **56** 046008